Non-rigid contour-to-pixel registration of photographic and quantitative light-induced fluorescence imaging of decalcified teeth

Benjamin Berkels[a], Thomas Deserno[b], Eva E. Ehrlich[c], Ulrike B. Fritz[c], Ekaterina Sirazitdinova[b], and Rosalia Tatano[a]

[a]AICES Graduate School, RWTH Aachen University, Schinkelstr. 2, 52062 Aachen, Germany
[b]Department of Medical Informatics, Uniklinik RWTH Aachen University, Pauwelsstr. 30, 52057 Aachen, Germany
[c]Department of Orthodontics, Uniklinik RWTH Aachen University, Pauwelsstr. 30, 52057 Aachen, Germany

ABSTRACT

Quantitative light-induced fluorescence (QLF) is widely used to asses the damage of a tooth due to decalcification. In digital photographs, decalcification appears as white spot lesions, i.e. white spots on the tooth surface. We propose a novel multimodal registration approach for the matching of digital photographs and QLF images of decalcified teeth. The registration is based on the idea of contour-to-pixel matching. Here, the curve, which represents the shape of the tooth, is extracted from the QLF image using a contour segmentation by binarization and morphological processing. This curve is aligned to the photo with a non-rigid variational registration approach. Thus, the registration problem is formulated as minimization problem with an objective function that consists of a data term and a regularizer for the deformation. To construct the data term, the photo is pointwise classified into tooth and non-tooth regions. Then, the signed distance function of the tooth region allows to measure the mismatch between curve and photo. As regularizer a higher order, linear elastic prior is used. The resulting minimization problem is solved numerically using bilinear Finite Elements for the spatial discretization and the Gauss-Newton algorithm. The evaluation is based on 150 image pairs, where an average of 5 teeth have been captured from 32 subjects. All registrations have been confirmed correctly by a dental expert. The contour-to-pixel methods can directly be used in 3D for surface-to-voxel tasks.

Keywords: Contour-to-pixel registration, image registration, QLF, Gauss-Newton minimization

1. INTRODUCTION

During orthodontic treatment with fixed devices, the mineral loss due to plaque accumulation on a tooth, called *demineralization*, is considered an iatrogenic, undesirable side effect. The presence of braces makes it considerably more difficult for the patient to reach some areas with a toothbrush.[1] In case of insufficient oral hygiene or repeated plaque accumulation, the risk of dental hard tissue damage increases in the form of so-called *white spot lesions* (WSL), which in digital photographs appear as chalky-white, opaque enamel areas.[2] In addition to aesthetic impairment, WSIs are characterized by mineral loss[3] and are considered preliminary stage of incipient caries (initial lesion). The quantitative light-induced fluorescence (QLF) provides information on both the qualitative as well as quantitative extent of demineralization.[4] In QLF images, demineralization appears as dark areas on the tooth surface.

Here, we propose a multimodal image registration approach for digital photos and QLF images of decalcified teeth (Fig. 3), based on a contour-to-pixel approach. A curve that represents the shape of a tooth is extracted from the QLF image and aligned to the tooth area shown in a digital photograph of the same tooth, by finding a non-rigid deformation that matches the curve to the boundary of the tooth in the photo. A non-rigid registration

Further author information: (Send correspondence to R.T.)
R.T.: E-mail: tatano@aices.rwth-aachen.de, Telephone: +49 (0)241 80 99 140

Medical Imaging 2016: Image Processing, edited by Martin A. Styner, Elsa D. Angelini, Proc. of SPIE Vol. 9784, 97840Z · © 2016 SPIE
CCC code: 1605-7422/16/$18 · doi: 10.1117/12.2216250

approach is required to correct the different view angles of the two images, which are due to their different manual acquisition methods. The registration of the two images allows to compare the demineralized areas shown by both modalities and thus to investigate whether the fusion of the two modalities can be beneficial in orthodontic treatment.

2. METHOD

2.1 Curve extraction

QLF segmentation aims at the extraction of the investigated tooth's contour. The task of QLF segmentation has not been widely addressed before. Hope et al. manually draw the contour of interest around the boundary of the tooth to asses the region of interest (ROI),[5] while Mansoor et al.[6] present their tool for semi-automatic QLF segmentation based on Gaussian Markov random field (GMRF). However, fully-automatic teeth segmentation raises several challenges. First, the border between tooth region and gum is not always sharp enough, interim demineralized regions often exhibit sharp edges instead. Second, there is usually more than one tooth visible in a QLF image and the borders between adjacent teeth are not always clearly defined by changes in intensity. To overcome those challenges, we combine a threshold-based method with an edge-based technique.

For the threshold-based part, the scaled down version of original image is split into two copies. The first copy is transformed from the red, green, blue (RGB) color space into the $I_1I_2I_3$ color space[7] and the component I_3 is taken for further processing. The component I_3 is invariant to intensity changes,[8] which allows us to retrieve a more regular silhouette of the teeth. A local adaptive Otsu threshold is applied to the resulting image to binarize it. The second copy of the original image is simply split into RGB channels. The blue channel is omitted as the QLF images tend to have only two colors: green – for healthy tooth regions, red – for damaged ones. We binarize the red and green channel images via a global Otsu threshold. Morphological holes filling and watershed are then applied to all three resulting images (binarized I_3, R and G channels) to respectively reduce the negative impact caused by the presence of lesion spots on the teeth silhouettes and get a rough separation of the teeth from each other. Then, the central tooth is extracted from each image. Finally, we combine the resulting images with the central tooth in one by pixel-wise summation. We have observed that combining those three images instead of using just one of them separately leads to a more precise silhouette detection. Finally, to eliminate the small holes left after joining the images, we successively apply morphological closing, holes filling and dilation.

The edge-based part is introduced for further improvement of the silhouette. To this end, Canny edge detection is applied to the original QLF image. Short isolated edges usually correspond to undesired structures. Thus, we remove all isolated edge pieces shorter than $\frac{1}{6}$ of the longest image dimension from the original edge image. Then, the morphological operators closing, dilation and skeletonizing are applied to fill gaps between the remaining edge pieces. Next, the impact of undesired structures is further reduced by removing edges shorter than $\frac{2}{9}$ of the longest edge in the image. The resulting image is then dilated.

Lastly, the edge image is subtracted from the threshold image. The resulting image, in turn, is processed with morphological erosion, holes filling and watershed. After all these steps the contour of the central element is extracted for further matching. Figure 1 illustrates the steps of the procedure.

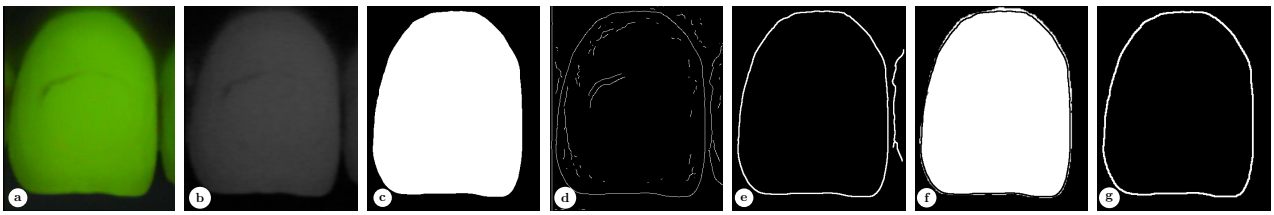

Figure 1. Input data. From left to right: (a) QLF image, (b) feature I_3 from the $I_1I_2I_3$ color space, (c) morphologically filtered sum of binarized I_3, R and G channels, (d) Canny edge image, (e) Canny edge image with short edges removed enhanced by morphological operations, (f) the resulting edge image subtracted from the resulting binary image and (g) detected tooth contour.

2.2 Photo pre-processing

To align the extracted curve to the tooth shown in the photo, the photo is first classified into tooth and non-tooth regions. This is achieved in three steps: first the photo is converted into a grayscale image, the resulting image is then segmented and finally thresholded.

Extracting the tooth region S_f directly from the photograph is difficult since typical RGB images show no clear distinction between the white of the tooth and the color of the gum. The contrast of tooth and gum can be significantly enhanced by switching to a more appropriate color space. Thus, we convert the image to the YC_bC_r color space via

$$Y = w_R R + (1 - w_B - w_R)G + w_B B, \quad C_b = \tfrac{0.5}{1-w_B}(B - Y), \quad C_r = \tfrac{0.5}{1-w_R}(R - Y),$$

where $w_R = 0.299$, $w_B = 0.114$ and $w_C = 0.587$.[9] Here, Y is the luminance component, C_b and C_r are the blue-difference and red-difference chroma components, and R, G and B are the red, green and blue components of f. To further enhance the contrast between the different regions of the YC_bC_r image, a new single channel image f_{prod} is created by multiplying the components via $f_{\text{prod}} = Y(1 - C_b)(1 - C_r)$ (Fig. 2). Then, f_{prod} is segmented using a four-phase Mumford-Shah segmentation[10] and thresholded using the intensity values of these regions in such a way that the points of the two regions with higher intensity values correspond to the tooth region denoted by S_f and the points of the other two correspond to the complement of S_f.

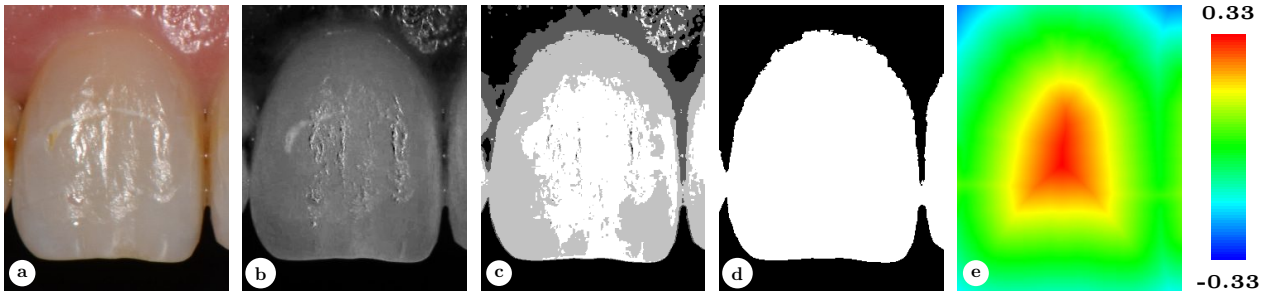

Figure 2. Input data. From left to right: (a) photo, (b) product image f_{prod}, (c) segmented f_{prod} and (d) tooth region S_f and (e) signed distance function of S_f visualized using blue-to-red color coding.

2.3 Mathematical model

Let us assume that we are given a digital photo, i.e. an RGB image and a QLF image of a tooth. We assume also that a curve $\mathcal{C}$ that represents the shape of the tooth is extracted from the QLF image (Sect. 2.1) and that the photo f is pointwise classified into tooth and non-tooth regions (Sect. 2.2). Let the curve $\mathcal{C}$ be given as set of points $\mathcal{C} = \{(x_i, y_i)\}_{i=1}^N = \{c_i\}_{i=1}^N$, where N is the number of points, and the RGB image f be given as mapping $f : \Omega \to \mathbb{R}^3$, where $\Omega = [0, 1]^2$. Furthermore, let $S_f \subset \Omega$ denote the part of the image classified as tooth (Fig. 2).

The registration method aims at finding a non-rigid deformation $\phi : \Omega \to \mathbb{R}^2$ that matches the curve $\mathcal{C}$ to the boundary of the tooth set $S_f \subset \Omega$. The alignment is attained by minimizing an energy that measures the distance of the deformed curve to the boundary of the tooth set and the smoothness of the deformation. The energy is

$$E[\phi] = E_{\text{match}}[\phi] + E_{\text{reg}}[\phi] = \frac{1}{2}\sum_{i=1}^{N} w_i \left(d(\phi(c_i), S_f)\right)^2 + \frac{\lambda^2}{2}\int_\Omega \|\Delta\phi(x)\|^2 \mathrm{d}x.$$

Here, $\lambda > 0$ is a parameter that controls the smoothness of ϕ, $w_i > 0$ are weights controlling the influence of the point c_i, and d is the signed distance function of S_f, i.e. $d(c, S_f) = \pm\text{dist}(c, \partial S_f)$ is the Euclidean distance of the point c to the boundary of S_f, where the sign is positive if c is outside of S_f and negative otherwise (Fig. 2).[11] The data term involves only the displacement of the curve points. However, the choice of a higher order regularizer allows the non-rigid deformation to be obtained on the whole domain of the digital photo. Thus, the whole photo is aligned to the QLF image.

Generally, there is no clear separation between a tooth and its neighbors (Fig. 2). Thus, the curve points on the vertical boundaries of the tooth may have no counterpart in the boundary of S_f. This issue is handled using the weights w_i. The vector $\vec{v}_i = \frac{1}{2}(c_{i+1} - c_i) + \frac{1}{2}(c_i - c_{i-1}) = \frac{1}{2}(c_{i+1} - c_{i-1})$ characterizes the orientation of the curve . The bigger the absolute value of the x-component of $\frac{\vec{v}_i}{|\vec{v}_i|}$, the less vertical is C at c_i. Hence, w_i it set to this value.

2.4 Discretization and minimization

The deformation ϕ is expressed as displacement $u = (u_1, u_2) : \Omega \to \mathbb{R}^2$ via $\phi(x) = x + u(x)$, for $x \in \Omega$. The image domain Ω is discretized with a uniform rectangular grid and u is discretized using bilinear Finite Elements on the grid.[12] Let J denote nodal index set and $\{\psi_j\}_{j\in J}$ the FE basis functions. Let M denote the lumped mass matrix and L the stiffness matrix, i.e. $M_{i,j} = \int_\Omega I(\psi_i\psi_j)\mathrm{d}x$ and $L_{i,j} = \int_\Omega \nabla\psi_i\nabla\psi_j\mathrm{d}x$, where I is the bilinear Lagrangian interpolation. Even though the regularizer involves second derivatives, it can be approximated with bilinear elements using these matrices via $E_{\mathrm{reg}}[u] = \frac{\lambda^2}{2}\sum_{i=1}^{2} \|M^{\frac{1}{2}}LU_i\|^2$.[13] Here, U_i is the vector of nodal values that uniquely represents the FE function u_i.

Using $F[u] = \left[\{\sqrt{w_i}d(c_i + u(c_i))\}_{i=1,\ldots,N}, \lambda M^{-\frac{1}{2}}LU_1, \lambda M^{-\frac{1}{2}}LU_2\right]^T$, we get $E[u] = \frac{1}{2}\|F[u]\|^2$. Thus, minimizing E is a nonlinear least square problem and can be solved efficiently using the Gauss-Newton method.[14] Local minimization methods like Gauss-Newton rely on a reasonably good initial guess. To this end, we first perform a regularized parametric registration,[15] using the affine deformation $\varphi(c) = Ac + t$, where A is 2×2 matrix and t a translation vector, the same data term as the non-rigid model and the Dirichlet energy as prior for the deformation, since the Laplacian of an affine deformation vanishes. Moreover, we use a coarse-to-fine matching to avoid that the minimization gets stuck in local minima, by solving the non-rigid registration problem for decreasing values of the parameter λ.

2.5 Data acquisition

All photographs were acquired with a digital SLR (Nikon D7000, Japan) under standardized conditions. A macro lens (Nikkor 105mm, 1: 2.8) with a ring flash (Sigma EM-140 DG) was used. The QLF images were recorded using the InspektorPro system (Panasonic WV-KS 152 QLF|clin, QLF software version 2.0.0.49, Inspector Research System BV, The Netherlands). The camera was integrated into a toothbrush handle. A xenon lamp (13mW/cm^2) with a wavelength of 370 ± 80 nm was used to reflect the light via the toothbrush handle on the surface of the tooth to be examined. The detection of the emitted fluorescence light was performed via a filter, where the effective detected light had a wavelength of 520 nm. In total, 150 QLF / photograph image pairs were acquired from 32 patients after brace removal. Figure 3 shows six of these QLF / photograph image pairs.

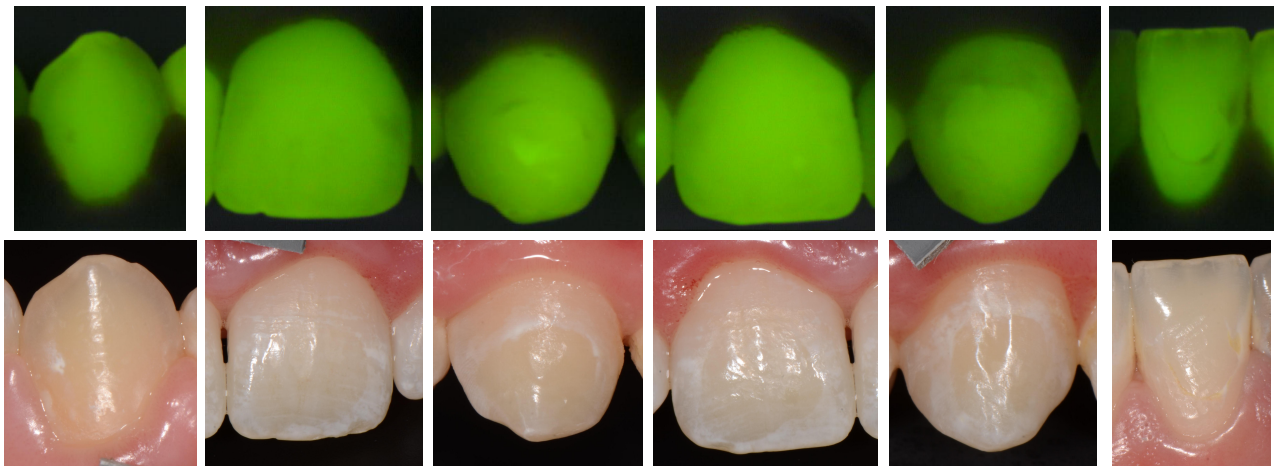

Figure 3. Input image pairs for six teeth: QLF images (top) and digital photographs (bottom).

3. RESULTS

Figure 4 depicts the results of the parametric and non-rigid registration applied to the six image pairs shown in Figure 3. The proposed method was applied to all 150 images pairs with empirically determined standard parameters. In particular, $\lambda = 1$ is used for the parametric registration and $\lambda = 10^{-i}$, $i = \{1, 2, 3\}$ were used for the non-rigid registration step. Since a ground-truth image was not available, the correctness of the registration was assessed by visual inspection of dental experts. The visual inspection revealed that the proposed registration method achieved reasonable results on 129 of the 150 images.

In the remaining 21 cases, the curve extracted from the QLF images was incorrect or not accurate, since part of the decalcified area was laying outside the extracted contour. In fact, extracting the tooth shape from the QLF images is not a simple task. Often, the presence of a decalcified area or the low contrast between the tooth and the black of the background makes difficult to find the correct contour of the tooth. Figure 5 presents 5 of the 21 cases in which the curve extraction method fails or the contour is not accurate. In most of these cases, the proposed contour-to-pixel method is capable of matching the extracted curve to the tooth region shown in the photo. However, the inaccuracy of the tooth contour leads to a registration that is not accurate enough to compare the decalcified area shown by two modalities.

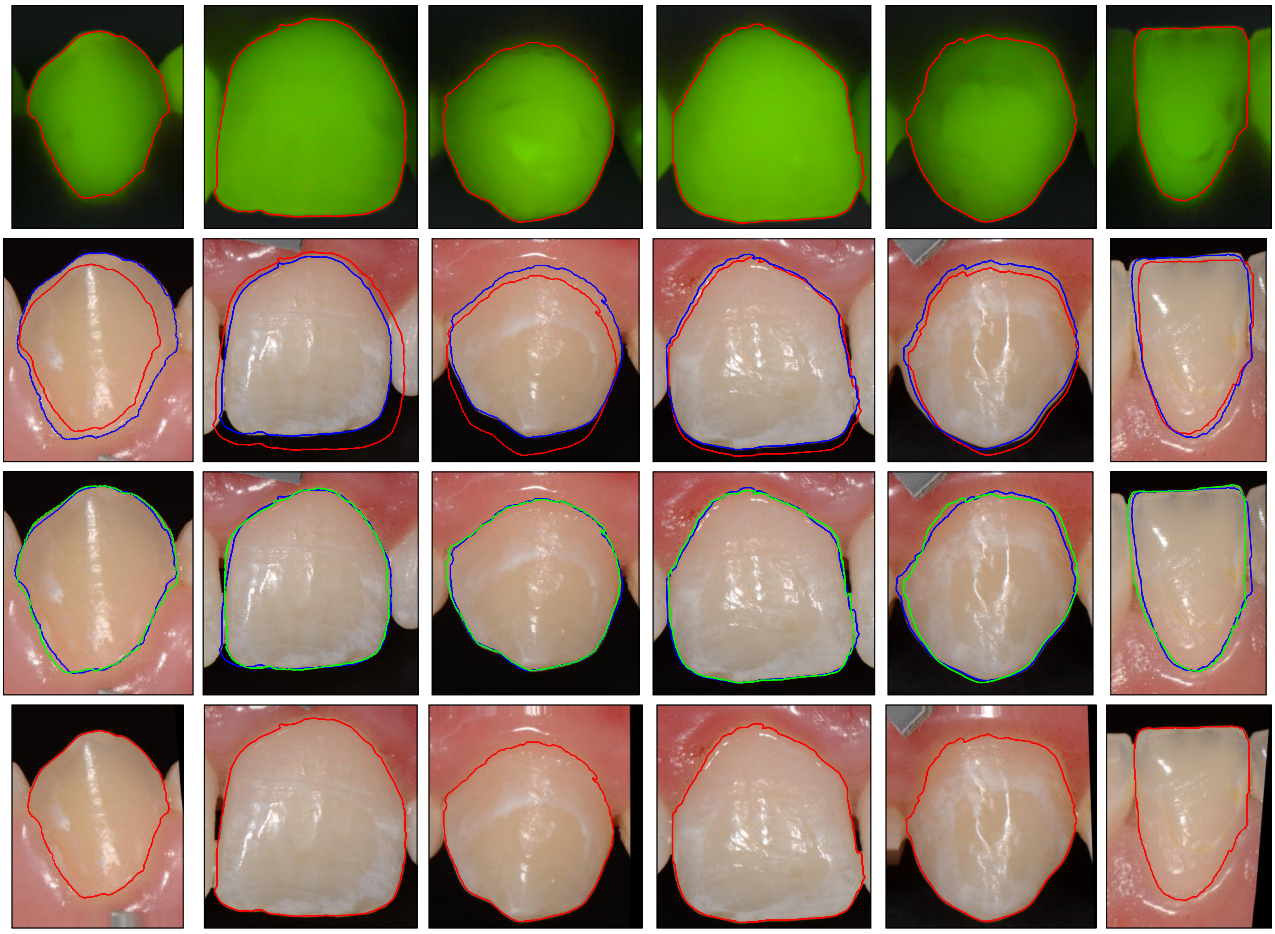

Figure 4. Results for six image pairs. From top to bottom: QLF image with the segmented curve (red), photo with the initial QLF curve (red) and the curve after the parametric registration (blue), photo with the curve after parametric registration (blue) and curve after the non-rigid registration (green), and photo deformed with the non-rigid deformation and the initial QLF curve (red).

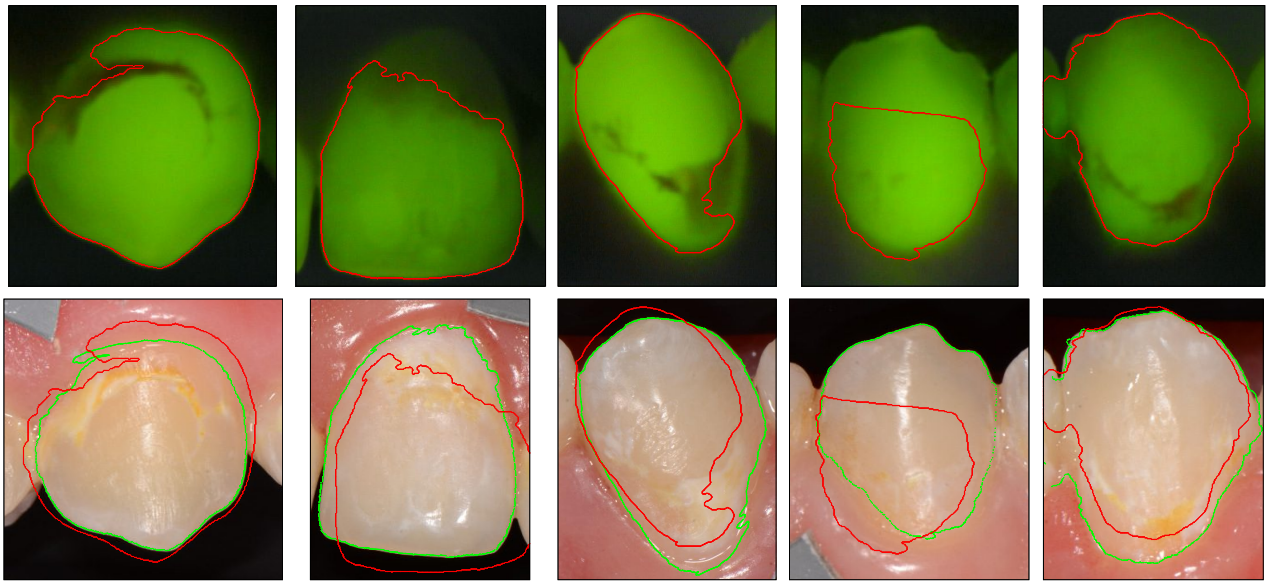

Figure 5. Five of the 21 cases detected by visual inspection in which the curve extraction fails or is not accurate: QLF images with extracted contour (red) and photo with the initial QLF curve (red) and the curve after the non-rigid registration (green).

4. CONCLUSION

We have proposed a novel method for the registration of photographs and QLF images of human teeth based on contour-to-pixel matching. The method was successfully applied to real clinical images. In the future, we plan to improve the extraction of the contour of a tooth from the QLF images and use the proposed method to evaluate the relation between damages to the tooth shown by QLF and the white spot lesions shown on the photographs.

The proposed contour-to-pixel matching has a natural extension to surface-to-voxel matching, which allows to use the same ideas for multimodal 3D registration problems. For instance, this approach is well-fitting when a volumetric patient scan needs to be registered to a segmented atlas. The boundary surfaces of the atlas segments take the role of the curve while the volumetric patient scan replaces the photograph.

REFERENCES

[1] Ousehal, L., Lazrak, L., Es-Said, R., Hamdoune, H., Elquars, F., and Khadija, A., "Evaluation of dental plaque control in patients wearing fixed orthodontic appliances: a clinical study," *Int Orthod* **9**, 140–155 (2011).

[2] Gorelick, L., Geiger, A., and Gwinnett, A., "Incidence of white spot formation after bonding and banding," *Am J Orthod* **81**, 93–98 (1982).

[3] Palamara, J., Phakey, P., Rachinger, W., and Orams, H., "Ultrastructure of the intact surface zone of white spot and brown spot carious lesions in human enamel," *J Oral Pathol* **15**, 28–35 (1986).

[4] Srivastava, K., Tikku, T., Khanna, R., and Sachan, K., "Risk Factors and Management of White Spot Lesions in Orthodontics," *J Orthod Sci* **2**(2), 43–49 (2013).

[5] Hope, C., Wang, Q., Burnside, G., Adeyemi, A., Quenby, S., Smith, P., Higham, S., and Whitworth, M., "Assessing the association between oral hygiene and preterm birth by quantitative light-induced fluorescence," *Scientific World J* **2014**(374694), 1–9 (2014).

[6] Mansoor, A., Patsekin, V., Scherl, D., Robinson, J., and Rajwa, B., "A statistical modeling approach to computer-aided quantification of dental biofilm," *IEEE J Biomed Health Inform* **19**(1), 358–366 (2015).

[7] Ohta, Y., Kanade, T., and Sakai, T., "Color information for region segmentation," *Comput Vision Graph* **13**(3), 222 – 241 (1980).

[8] Mrak, M., Grgic, M., and Kunt, M., [*High-Quality Visual Experience: Creation, Processing and Interactivity of High-Resolution and High-Dimensional Video Signals*], Signals and Communication Technology, Springer Berlin Heidelberg (2010).

[9] Sridhar, S., [*Digital Image Processing*], Oxford University Press (2011).

[10] Zach, C., Gallup, D., Frahm, J., and Niethammer, M., "Fast global labeling for real-time stereo using multiple plane sweeps," in [*Proc Int Fall Workshop Vis Model Vis*], 243–252, Aka GmbH (2008).

[11] Bauer, S., Berkels, B., Hornegger, J., and Rumpf, M., "Joint ToF image denoising and registration with a CT surface in radiation therapy," in [*Lect Notes Computer Sci*], 98–109 (2011).

[12] Braess, D., [*Finite Elements: Theory, Fast Solvers, and Applications in Solid Mechanics 3rd Edition*], Cambridge University Press (2007).

[13] Berkels, B., Cabrilo, I., Haller, S., Rumpf, M., and Schaller, K., "Co-registration of intra-operative brain surface photographs and pre-operative MR images," *Int J Comput Assist Radiol Surg* **9**(3), 387–400 (2014).

[14] Gratton, S., Lawless, A. S., and Nichols, N. K., "Approximate Gauss-Newton methods for nonlinear least squares problems," *SIAM J Optim* **18**(1), 106 – 132 (2007).

[15] Chumchob, N. and Chen, K., "A Robust Affine Image Registration Method," *Int J Num Anal Model* **6**(2), 311–334 (2009).